Nuclear Instruments and Methods in Physics Research A 608 (2009) 410-416
doi:10.1016/j.nima.2009.07.022

A Digital X-ray Imaging System based on Silicon Strip Detectors working in Edge-on Configuration

L. Bolanos[a], M. Boscardin[b], A.E. Cabal[a], M. Diaz[c], P. Grybos[d], P. Maj[d], F. Prino[e], L. Ramello[f*], R. Szczygiel[d]

[a]CEADEN, Calle 30 #502 e/ 5ta y 7ma Avenida, Playa, Ciudad Habana, Cuba;
[b]IRST, Fondazione Bruno Kessler, Via Sommarive 18, Povo, 38100 Trento, Italy;
[c]InSTEC, Ave. Salvador Allende esq. Luaces, Quinta de los Molinos, Ciudad Habana, Cuba;
[d]Faculty of Electrical Engineering, Automatics, Computer Science and Electronics, Department of Measurement and Instrumentation, AGH University of Science and Technology, Al. Mickiewicza 30, 30-059 Cracow, Poland;
[e]Istituto Nazionale di Fisica Nucleare, Sezione di Torino, Via P. Giuria 1, 10125 Torino, Italy;
[f]Dipartimento di Scienze e Tecnologie Avanzate, Università del Piemonte Orientale, Via T. Michel 11, 15100 Alessandria, Italy.
*Correspondig author, e-mail: luciano.ramello@mfn.unipmn.it

Abstract – We present the energy resolution and imaging performance of a digital X-ray imaging system based on a 512-strip silicon strip detector (SSD) working in the edge-on configuration. The SSDs tested in the system are 300 μm thick with 1 or 2 cm long strips and 100 μm pitch. To ensure a very small dead area of the SSD working in edge-on configuration, the detector is cut perpendicular to the strips in a distance of only 20 μm from the end of the strips. The 512-strip silicon detector is read out by eight 64-channel integrated circuits called DEDIX (Grybos et al., 2007). The DEDIX IC operates in a single photon counting mode with two independent amplitude discriminators per channel. The readout electronic channel connected to a detector with effective input capacitance of about 2 pF has an average equivalent noise charge (ENC) of about 163 el. rms and is able to count 1 Mcps of average rate of input pulses. The system consisting of 512-channels has an excellent channel to channel uniformity - the effective threshold spread calculated to the charge sensitive amplifier inputs is 12 el. rms (at one sigma level). With this system a few test images of a phantom have been taken in the 10-30 keV energy range.

Keywords – Silicon; strip; imaging; X-ray; amplifier.

1. Introduction

Digital imaging systems based on silicon strip/pixel detector are widely used in high energy physics experiments and X-ray imaging system [1]-[6]. However in case of X-ray imaging a standard 300 μm thick detector converts nearly all 8 keV X-ray, but only ~26.7% of 20 keV X-ray and ~2% of 60 keV X-ray. Therefore many laboratories are conducting intensive research on other semiconductor materials with higher atomic number (like CZT, GaAs etc) [7]-[8]. There are also groups who make an effort to build an effective imaging system for higher energy X-rays based on a silicon strip detector (SSD) in edge-on configuration with the mechanical scanning [9]-[15]. The quality of such an imaging system is determined by several parameters and among them the most important are: (i) the small dead area of a detector working in edge-on configuration and (ii) a low-noise multichannel readout electronics with high count rate performance and short dead time.
In the present paper we present experimental results of 512-channel system built around the DEDIX 64-channel ASIC [1]; preliminary results have been reported in [13].
We have already explored potential applications of this detector concept to dual energy medical imaging, namely dual energy mammography [15] and K-edge angiography [16], and also to the K-edge mapping of pigments in art paintings [17].
The paper is organized as follows. Section 2 describes the parameters of silicon strip used for operation in edge-on configuration. Section 3 is a short description of the DEDIX integrated circuit architecture

and the 512-channel modules. The measurement parameters obtained with these modules are presented in Section 4. Section 5 contains some examples of different images taken with this module and Section 6 summarizes the obtained results.

2. Silicon microstrip detector in edge-on configuration

Silicon microstrip detectors have reached technical maturity since many years, being widely used in high energy physics mainly for charged particle (MIP) tracking. In the case of imaging with X-rays of relatively low energy (10-60 keV) the main concerns are: efficiency, signal-to-noise ratio and rate capability. The last two points depend mainly on the performance of the front-end electronics (see next Section), though of course the strip leakage current and the strip capacitance impact on the noise level. The efficiency on the other hand depends on the detector geometry: the edge-on orientation helps to keep a high efficiency. However in conventional detector designs the dead layer between the strips and the physical edge (typically 500 μm) severely limits the efficiency at low energies.

In order to overcome this limit, we decided to implement the Current Terminating Structure (CTS) [18] developed for the Roman Pots of the TOTEM experiment at LHC, which allows one to obtain much reduced edge thickness. Figure 1 shows the computed efficiency for converting X-rays of energies up to 60 keV in edge-on geometry, for 1 cm and 2 cm strip length and for edge thicknesses of 20 μm and 60 μm. For comparison also the case of 1 cm strips and 500 μm edge is shown. The advantage of reduced edge thicknesses is evident in the 5-30 keV range, while the 2 cm length option is interesting particularly if the application requires energies around 50 keV (one such application is imaging at the Gd K-edge).

The basic parameters of our detectors are: p+ strip on n-type substrate of 300 μm thickness, strip pitch 100 μm. The detector is an AC coupled one with a punch-through bias structure. The detector leakage current measured for a few selected detectors is below 500 pA/strip after cutting at 20 μm (this is an average value which could be dominated by a few hot strips). The total strip capacitance is about 2 pF and 4 pF for the 1 cm and 2 cm strips, respectively. All detectors were designed and fabricated by FBK-IRST, Trento, Italy.

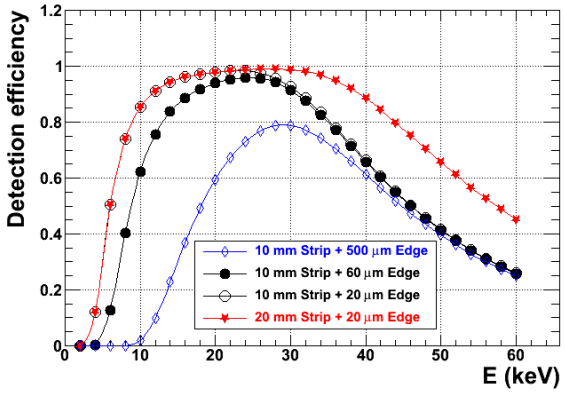

Fig. 1. Efficiency of conversion vs. X-ray energy for edge-on silicon detectors, with four choices of geometrical parameters.

A detail of the silicon strip detector layout is shown in Fig. 2, with a few strips, the guard ring and the Current Terminating Structure visible. Each wafer contained four large 512-strip detectors, three with 1 cm long strips and one with 2 cm long strips, as well as other conventional strip detectors and test structures. The large detectors were characterized by their I-V curves, both for bias line (I_{BL}) and guard ring (I_{GR}) currents, which were measured up to 100 V bias voltage, before and after wafer cutting at either 60 μm or 20 μm from the physical edge.

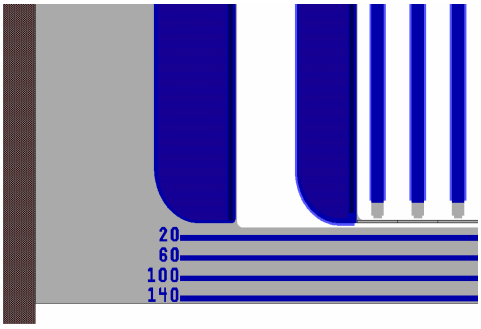

Fig. 2. Layout of a corner of the SSD designed for edge-on utilization, shown before cutting. X-rays will be incident from the bottom. In the upper part, from right to left: three strips, guard ring, Current Terminating Structure. Cut lines at four different distances from the sensitive region are visible in the lower part.

The current I_{GR} at 100 V was 1-2 mA after wafer cutting for all large detectors; the bias line current I_{BL} (sum over 512 strips) at 100 V showed instead huge variations, increasing of a factor between 2 and 9000 with respect to the uncut wafer value. We selected for further work three of the detectors showing the lowest values of I_{BL} after cut, which are quoted as module I (1 cm strips, 60 μm cut), module II (2 cm strips, 20 μm cut) and module III (1 cm strips, 20 μm cut) in the next sections. Their I_{BL} at 100 V after cut was in the range 100-200 nA.

3. Electronic read-out system

3.1 Architecture of the DEDIX integrated circuit

The DEDIX integrated circuit comprises six basic blocks (see Fig. 3(a)): 64 analog front-end channels, 2×64 counters, an input-output block, a control command decoder, control DACs and a calibration circuit. This integrated circuit (IC) is designed in the 0.35 μm Austriamicrosystems AG CMOS process and the layout total area is 3900×5000 μm^2. The block diagram of a single channel is shown in Fig. 3(b). Each channel is built of a charge sensitive amplifier (CSA) with a pole-zero cancellation (PZC) circuit, a CR-RC^2 shaper with a peaking time of 160 ns, two discriminators and two independent 20-bit counters. The threshold voltages for two discriminators (A and B) in a single channel are set independently, but are common for all 64 channels of the IC. Because from the CSA input up to the discriminator inputs the signal processing chain is DC-coupled, a correction DAC (working in each channel independently) is necessary to minimize the effects of the DC level spread at the discriminator inputs. A detailed description of the DEDIX IC can be found in [1].

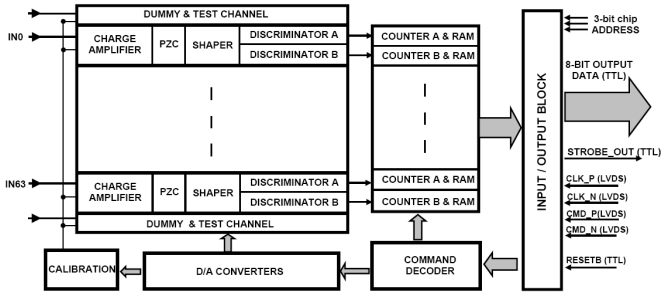

(a)

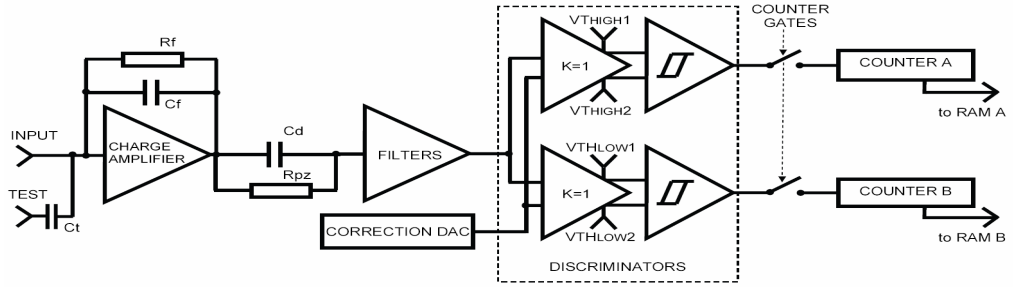

(b)

Fig. 3. The DEDIX Integrated Circuit: (a) block diagram, (b) scheme of a single channel.

3.2 Front-end modules

Three different 512-channel modules were built using silicon strip detectors in edge-on configuration: modules I, II and III as quoted in the previous section. Each module contains 8 DEDIX ICs which:
– in the case of modules I and II are connected to SSD having 1 or 2 cm long strips using a pitch adapter printed on a glass substrate – see Fig. 4(a),
– in the case of module III are connected directly to SSD having 1 cm long strips - see Fig. 4(b).

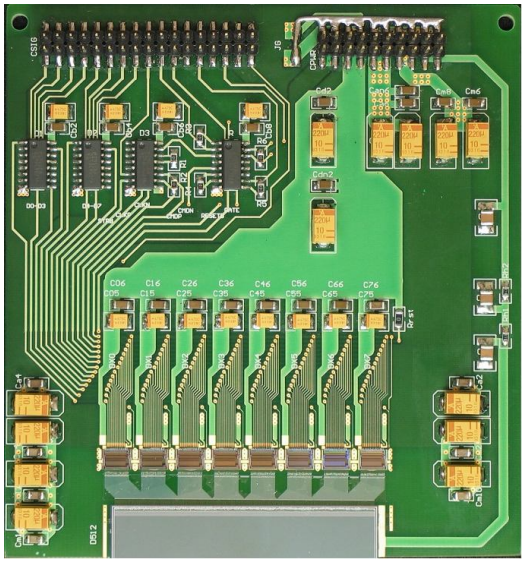

(a)

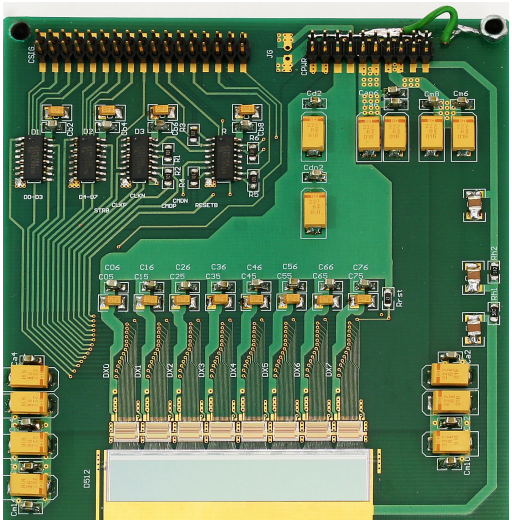

(b)

Fig. 4. Photographs of multichip modules with 512-silicon strip detector: (a) module I with 1 cm long detector with a glass pitch adapter, (b) module III with 1 cm long detector connected directly to ICs.

Module I is our first prototype, however because the pitch adapter adds some additional parasitic capacitance, a new printed circuit board (PCB) for module III was designed, which allows the direct bonding between the detector and the integrated circuits. The 6-layer PCB contains additional decoupling capacitors and low-voltage differential drivers (DS90LV031A) and receivers (DS90LV032A). Modules are controlled using a digital I/O card (National Instruments PCI 6534) plugged into a PC and all signals (clock, control and data) are transferred to or from the module using LVDS standard. Data are collected with a program written in LabVIEW 8.2 (National Instruments).

In this configuration a single module is a row of 512 pixels with dimensions 100 μm × 300 μm. To obtain a 2D image, a mechanical scan in the direction perpendicular to PCB plane is used.

4. Measurement of the main parameters of 512-channel modules

4.1 Effective threshold spread and noise

In the case of DEDIX IC two discriminators thresholds A and B are common for all channels. The critical aspect of such a solution is the channel to channel spread of the effective threshold levels. To compensate this variation a 7-bit correction DACs (implemented in each channel of the IC) is loaded at the system start-up. After loading the proper values of correction DACs, the spread of effective threshold voltage in discriminators A in our module, as measured with fluorescence X-rays, is equal to 1.33 mV rms for all the 512 channels. If 3 channels with higher offset (namely no. 123, 289 and 290 - see Fig. 5(a)) are excluded, the spread is reduced to 0.63 mV which, when referred to the input, corresponds to about 12 el. rms (at one sigma level).

The measured spread for the discriminators B (set 240 mV below threshold A) is of about 6 mV and there are two reasons for this higher value of the spread: (i) the correction DAC in each channel is common for discriminators A and B, which have different input offsets, and values of correction DACs are optimised for discriminators A; (ii) the variation of the gain from die to die - see Fig. 5(b).

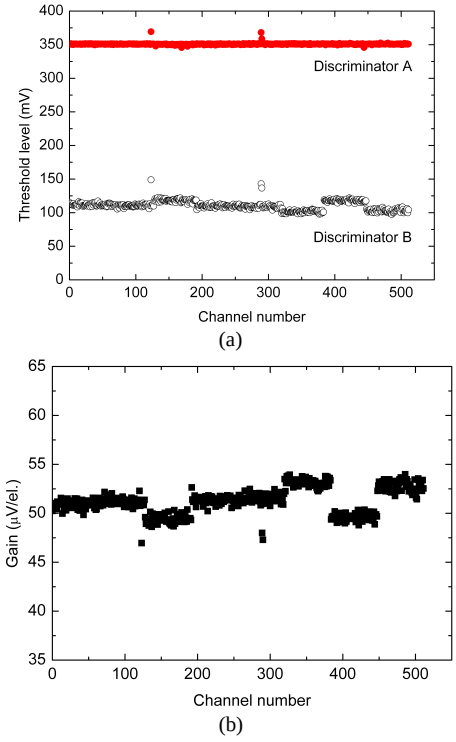

Fig. 5. (a) Spread of the effective threshold level for discriminators A set to average values of 350 mV and for discriminators B set at the same time to the average values of 110 mV. (b) Spread of the gain for module I.

For module I (with standard IC settings, power consumption 5 mW/channel) the mean gain is 51.2 μV/el. with standard deviation of 1.33 μV/el - see Fig. 5(b). Setting the discriminators B for different energy levels than discriminators A causes that the effective threshold spread for discriminators B in our system is mainly determined by the die-to-die variations of the gain.

The spread of the effective discriminators levels is similar in all three modules. The measured equivalent noise charges for the tested 512-channel systems are summarized in Table I. The average ENCs for modules I, II and III are respectively:

- 193 el. rms (1 cm SSD with pich adapter),
- 243 el. rms (2 cm SSD with picth adapter),
- 163 el rms (1 cm SSD without pitch adapter).

Module II was operated at the same gain as module I, while in the case of module III we used a different setting for lower current consumption (3 mW/channel), which resulted in an average gain of 38 μV/el.

TABLE I

NOISE PERFORMANCE OF 8 ASICS INSTALLED ON PCB

Chip Number	Module I ENC [el. rms]	Module II ENC [el. rms]	Module III ENC [el. rms]
1	185	(*)	160
2	190	239	164
3	188	242	165
4	208	245	163
5	206	244	165
6	199	245	160
7	179	245	161
8	188	255	166

(*) Chip was mechanically damaged during the measurements.

4.2 Energy resolution

The energy resolution of our system is determined by the noise performance of the readout electronics which is enough good for the foreseen applications. The small threshold spread in the system allows the effective photon counting in a given energy window. Two examples of measured energy spectra of Zr and Sn are shown in Fig. 6(a) and 6(b).

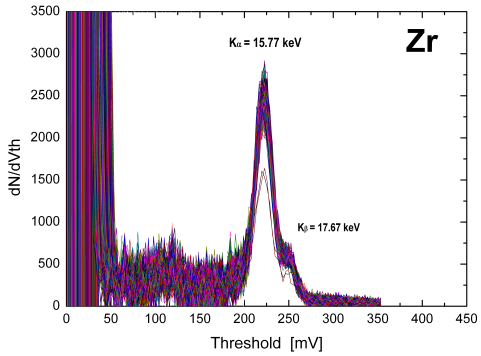

Fig. 6(a). Energy spectra measured in 509 channels of module I (edge-on configuration) using threshold scan for Zr fluorescence. Two channels with lower number of counts are situated on edge of the detector.

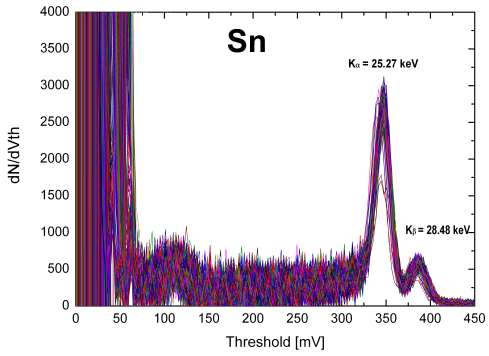

Fig. 6(b). Energy spectra measured in 509 channels of module I (edge-on configuration) using threshold scan for Sn fluorescence. Two channels with lower number of counts are situated on edge of the detector.

In the case of Sn spectra (see Fig. 6(b)) one can easily distinguish K_α and K_β peaks separated only by 3.2 keV.

For a system using mechanical scan to obtain 2D-imaging the important parameters are high count rate performance and short data readout time (dead time of the system). As it is shown in [1] the analog parameters of DEDIX IC do not degrade up to 1 Mcps of average rate of input pulses. Another important issue is the dead-time of the IC. After the exposure time the counter gates are switched off

(see Fig. 3.b), the values of 20-bit counters are loaded into RAMs and the counters are reset. With 30 MHz clock these operations last about 340 ns. This buffering scheme ensures that the data readout and counting of the input pulses can be performed simultaneously and no additional noise counts are registered in this mode. In the readout mode separate from exposure the readout time of single IC is 16.7 μs, and for the 8 chip module is of about 133 μs (with 30 MHz clock).

5. Imaging test

We acquired test images of the phantom sketched in Fig. 7 exploiting a mechanical scan with 300 μm step. The goal was to validate the concept of obtaining 2D images with our 1D strip detector using a monochromatic X-ray beam, rather than optimizing the signal-to-noise ratio.

The setup consisted of a 2 kW Cu-anode X-ray tube (maximum voltage 60 kV, maximum current 60 mA for voltages up to 30 kV, 50 mA for 40 kV), a set of interchangeable fluorescence targets (oriented at 45° with respect to the primary beam, dimensions 25 by 25 mm^2), a secondary beam at 90° with respect to the primary beam, a phantom and a silicon strip detector**.**

The phantom consisted of a plexiglass slab 5.6 mm thick, with various hollows and inserts (see Fig. 7); it was mounted on a moving holder placed at 60 cm from the fluorescence target, perpendicular to the secondary beam.

The silicon strip detector (module III) was in a fixed position at 70 cm from the target, with edge-on orientation (strips parallel to the secondary beam); a sensitive region 300 μm wide (detector thickness) and 51.2 mm high (512 strips) was then available. Due to the distance between the target and the detector, the secondary beam flux was rather uniform along the 512 strips. A flat-field correction was applied to the raw images.

The images were obtained by moving the phantom across the detector with a step equal to the detector thickness; a pixel of the following images is therefore 300 μm by 100 μm. The typical acquisition time was 40 s per scanning step, i.e. a total time of 80 minutes for 120 steps, limited by the low luminosity of fluorescence X-rays in our set-up: 2500 counts/mm^2/s or about 75 counts/pixel/s. Images were processed using the ROOT framework [19].

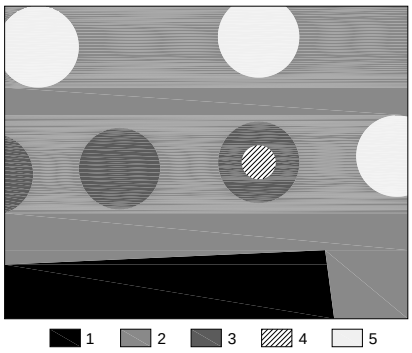

Fig. 7. Front view of the phantom (only the imaged area, about 51 mm × 36 mm). Region 2 (the body) is a plexiglass slab 5.6 mm thick. Cylindrical hollows 2.95 mm deep machined in the plexiglass contain either wax (region 3) or air (region 5). Inside the wax there is a thin aluminium foil (region 4) of thickness 75 μm. Region 1 is a brass foil used for alignment purposes.

Figure 8(a) shows the final image obtained with the highest fluorescence energy available in our setup, namely that of Sn, with K_α peak at 25.3 keV and K_β peak at 28.5 keV. Thresholds A and B were set such that we could use discriminators B counts to subtract the Sn-K_β contribution from the final image, which is therefore an image at 25.3 keV. It is evident that the contrast is not very good and the Al insert within the wax is barely visible. Numerical values of contrast between different regions i and j (defined in Fig. 7) are reported in Table II; the contrast is defined as $(C_i-C_j)/C_2$ where C_i and C_j are the averages of counts in region i and j (so the contrast is always normalized to the counts in region 2), and its error is defined as $\sqrt{(rms_i^2-rms_j^2)}/C_2$.

Figure 8(b) shows the final image obtained with a lower fluorescence energy, namely that of Zr, with K_α peak at 15.8 keV and K_β peak at 17.7 keV. Since this K_β peak cannot be resolved by our system (see Fig. 6(a)), we set the threshold of discriminators B just above the Zr K_β peak, in order to subtract the counts due to continuum photons at higher energies. In the case of Fig. 8(b) the contrast is much better than Fig. 8(a), and the Al insert is clearly visible. Numerical values of contrast between different regions are again reported in Table II.

Finally, Fig. 8(c) shows the final image obtained with the lowest fluorescence energy, namely that of Ge. Since the K_β peak of Ge cannot be resolved by our system, we set the threshold of discriminators B just above the K_β peak, in order to subtract the counts due to continuum photons at higher energies. In the case of Fig. 8(c) the contrast (Table II) is even better than Fig. 8(b), and the Al insert is clearly visible.

Signal-to-noise ratios (SNR) are presented for the three images in Table III. SNR is defined as $(C_i - C_j)/rms_2$ where C_i and C_j are the counts (corrected for flat-field) in ROIs of size 10×10 pixels defined in regions i and j (defined in Fig. 7) and rms_2 is the rms fluctuation of the counts in region 2, defined with a 1×1 pixels noise sampling area. The air-plexiglass SNR is in each case acceptable (i.e. greater than 5 as dictated by the Rose criterion), while the Al-wax SNR is barely acceptable only for the case of Ge target. It must be noted that the latter image suffers from lower statistics with respect to other images (counts in the plexiglass region for Ge target are only about 1/4 with respect to Sn and Zr ones) and this is especially visible in the SNR values between regions 2 and 3.

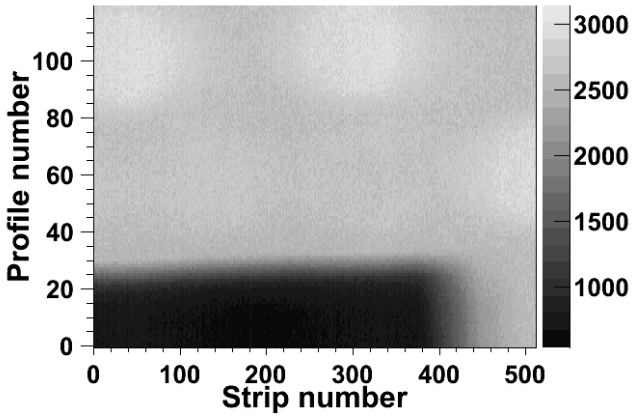

(a)

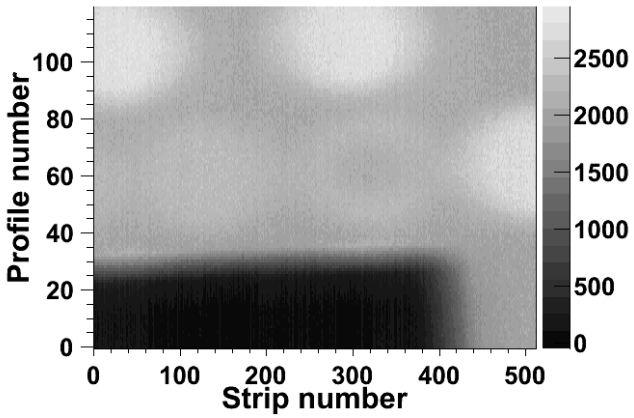

(b)

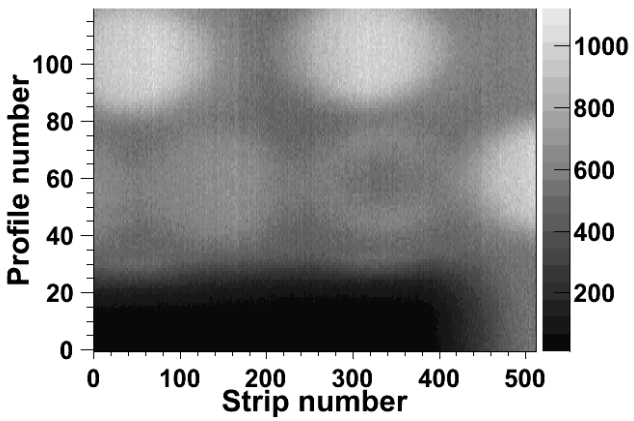

(c)

Fig. 8. Images of the phantom (horizontal axis: 512 strips at 100 μm pitch; vertical axis: 120 scanning steps at 300 μm pitch) collected with fluorescence X-rays from: (a) Sn target – K_α peak at 25.3 keV, K_β peak at 28.5 keV; (b) Zr target – K_α peak at 15.8 keV, K_β peak at 17.7 keV; (c) Ge target – K_α peak at 9.9 keV, K_β peak at 11.0 keV. The scales of grays on the right-hand side of each image represent the counts, corrected for flat-field.

TABLE II

CONTRAST BETWEEN DIFFERENT PARTS OF THE IMAGES

Regions involved	Sn image contrast	Zr image contrast	Ge image contrast
2-5	0.118±0.030	0.329±0.037	0.692±0.074
2-3	0.024±0.028	0.111±0.038	0.115±0.077
3-4	0.024±0.027	0.104±0.037	0.238±0.067

TABLE III

SIGNAL-TO-NOISE RATIO IN DIFFERENT PARTS OF THE IMAGES

Regions involved	Sn image SNR	Zr image SNR	Ge image SNR
2-5	5.95	11.6	13.6
2-3	1.20	3.90	2.26
3-4	1.21	3.65	4.68

We have not fully exploited the high rate capability of our system, namely 1 Mcps per channel (see previous section); for this purpose, dedicated 2D imaging tests with higher flux of X-rays at a synchrotron facility [10] or with a dual energy setup [20,21] would be appropriate. A factor 1000 increase of the counts/pixel/s can be anticipated, reducing the acquisition time quoted earlier from 80 minutes to 5 seconds.

The obtained system performance and the imaging test suggest that our 512-strip modules can find useful applications, among others, in digital radiography – both dual energy mammography [15] and angiography with the K-edge subtraction technique [18] - and in the mapping of pigments of art paintings [17]. The K-edge subtraction technique requires two such modules placed a few mm apart, respectively dedicated to energies below and above the K-edge; energies of interest range from about 10 keV up to 50 keV (Gd K-edge). In the case of dual energy mammography, the two energy components of the beam will be detected by a single module, thanks to the availability of discriminators A and B.

6. Summary

We have presented a 512-channel module based on Silicon Strip Detectors working in edge-on configuration with a very small dead area of the detector. The comparison of our system with other systems working with silicon strip detector in edge-on configuration is presented in Table IV.

The noise, channel-channel uniformity and count rate performance make the system promising for 2-D imaging in the range of low and medium energy range of X-rays. Images of a phantom taken with fluorescence X-rays at different energies demonstrate the imaging capabilities of the system in edge-on configuration even at low X-ray energies.

TABLE IV

COMPARISON OF SYSTEMS WORKING WITH SILICON STRIP DETECTOR IN EDGE-ON CONFIGURATION

Reference	[11,22]	[9, 23]	[12]	[14,15]	This work
Strip pitch × detector thickness [μm × μm]	100 × 300	500 × 500	100 × 300	100 × 300	100 × 300
Dead layer of detector [μm]	-	-	240	765	20
Number of channels	16	1000	384	384	512
Noise [el. rms]	40	190[a]	500	200	163
Shaper peaking time [ns]	50[b]	500	75	800	160
Max count rate per channel [MHz]	2	-	3.5	0.1	1
Threshold spread - std dev [el.]	300	24.5	-	87	12
Energy window	no	yes	no	yes	yes

[(a)] noise without detector

[(b)] minimum peaking time

Acknowledgements

The authors are grateful to M. Gambaccini from University of Ferrara for providing the phantom. The authors from the AGH University of Science and Technology gratefully acknowledge the opportunity to be a member of the Cadence Academic Network, providing us with a very valuable knowledge and methodology exchange plat-form. We gratefully acknowledge Floreana Dumitrache and Barbara Pini from INFN Torino and Maciej Kachel from AGH UST Cracow for their careful bonding work.

This work was supported by Ministry of Science and Higher Education, Poland and Istituto Nazionale di Fisica Nucleare, Italy.

References

[1] P. Grybos, et al.: "Measurements of Matching and High Count Rate Performance of Multichannel ASIC for Digital X-Ray Imaging." *IEEE Trans. Nucl. Sci,*. vol. 54, 2007, pp. 1207-1215.

[2] X. Llopart, M. Campbell, R. Dinapoli, D. San Segundo, E. Pernigotti, "Medipix2: a 64-k Pixel Readout Chip With 55-μm Square Elements Working in Single Photon Counting Mode.", *IEEE Trans. Nucl. Sci.,* vol. 49, no. 5, 2002, pp. 2279 - 2283.

[3] Ch. Bronnimann, et al.: "A pixel read-out chip for PILATUS project." *Nucl. Instrum. Methods A*, vol. 465, 2001, pp. 235-239.

[4] R. Rossi, P. Fischer, T. Rohe, N. Wermes "Pixel Detectors. From Fundamentals to Applications", Springer-Verlag, Berlin, Heidelberg 2006.

[5] Y. Allkofer et al., "Design and performance of the silicon sensors for the CMS barrel pixel detector" *Nucl. Instrum. Methods*, vol. A584, 2008, pp. 25–41.

[6] H.J. Simonis, "Status of the silicon strip detector at CMS" *Nucl. Instrum. Methods*, vol. A598, 2009, pp. 46–49.

[7] G. De Geronimo, P. O'Connor, J, Grosholz "A generation of CMOS readout ASICs for CZT detector." *IEEE Trans. Nucl. Sci.,* vol.47, no.6, pp. 1857-1876, Dec. 2000.

[8] L. Tlustos et al., "Characterisation of an epitaxial GaAs/Medipix2 detector using fluorescence photons" *Nucl. Instrum. Methods*, vol. A591, 2008, pp. 42–45.

[9] B. Hilt, P. Fessler, G. Prevot, "New quantum detection system for very low dose X-ray radiology." *Nucl. Instrum. Methods*, vol. A442, 2000, pp. 38–44.

[10] C. Venanzi, A. Bergamaschi, D. Derossi, S. Olivo, S. Pani, R. Longo, et al., "A digital detection system for synchrotron radiation breast tomography" *IEEE NSS-MIC 2004 Conference Record*.

[11] E. Beuville, R. Cahn, B. Cederstrom, M. Danielsson, A. Hall, B. Hasegawa, et al., "High resolution X-ray imaging using a silicon strip detector." *IEEE Trans. Nucl. Sci.,* vol.45, no.6, pp. 3059-63, Dec. 1998.

[12] E. Verbitskaya, et al., "Advanced Model of Silicon Edgeless Detector Operation" *IEEE NSS-MIC 2008 Conference Record*, pp. 2711-2716.

[13] L. Ramello, et al.: "Development of a 512-channel Module for Digital X-ray Imaging Systems with SSD" *Poster P3-17 presented at the Xth EFOMP Congress – First European Conference on Medical Physics*, Castelvecchio Pascoli, Italy, 20-22 September 2007

[14] P. Grybos, et al.: "RX64DTH - A fully integrated 64-channel ASIC for a digital X-ray imaging system with energy window selection." *IEEE Trans. Nucl. Sci,*. vol. 52, 2005, pp. 839-846.

[15] C. Avila et al., "Contrast cancellation technique applied to digital x-ray imaging using silicon strip detectors", Med. Phys. 32 (2005) 3755-3766.

[16] A. Sarnelli et al., "K-edge digital subtraction imaging based on a dichromatic and compact x-ray source" *Phys. Med. Biol.* 49 (2004) 3291-3305.

[17] P. Baldelli et al.: "Application of the K-edge X-ray technique to map pigments of art paintings: Preliminary results" *Nuovo Cim.*, vol. 29C, 2006, pp. 663-672.

[18] G. Ruggiero et al.: "Planar edgeless silicon detectors for the TOTEM experiment" *IEEE Trans. Nucl. Sci,*. vol. 52, 2005, pp. 1899-1902.

[19] R. Brun and F. Rademakers, "ROOT – An Object Oriented Data Analysis Framework" *Nucl. Instrum. Methods*, vol. A389, 1997, pp. 81–86; see also http://root.cern.ch
[20] M. Gambaccini et al.: "Narrow energy band x-rays via mosaic crystal for mammography application" *Nucl. Instrum. Methods*, vol. A365, 1995, pp. 248–254.
[21] A. Tuffanelli et al.: "Evaluation of a dichromatic x-ray source for dual-energy imaging in mammography" *Nucl. Instrum. Methods*, vol. A489, 2002, pp. 509–518.
[22] E. Beuville et al.: "An application specific integrated circuit and data acquisition system for digital X-ray imaging" *Nucl. Instrum. Methods*, vol. A406, 1998, pp. 337–342.
[23] P. Fessler et al.: "An important step forward in continuous spectroscopic imaging of ionising radiations using ASICs" *Nucl. Instrum. Methods*, vol. A421, 1999, pp. 130–141.